

## Detection and modification of DNA supercoiling

Arinbjörn Kolbeinsson

Supervised by Dr Tom Ellis and Dr Olivier Borkowski

Department of Bioengineering  
Imperial College London

June 16<sup>th</sup>, 2015

### Abstract

---

Genetic transcription events cause the surrounding DNA to supercoil. This results in modified expression of neighbouring genes. I designed and built three constructs to quantify supercoiling under given conditions. I did this to improve both our understanding of the supercoiling mechanism and the design of future biological parts for synthetic biology. The  $P_{\text{gyrA}}$  promoter was used as a detector of supercoiling but its response did not match those presented in the literature. I inserted a topological insulator upstream of the  $P_{\text{gyrA}}$  promoter to reduce the supercoiling level. The insulator did not reduce the  $P_{\text{gyrA}}$  activity, possibly because  $P_{\text{gyrA}}$  promoter activity did not increase with supercoiling. Under the same conditions, a constitutive promoter showed decreased induction as the supercoiling density increases, relative to a control. This result suggests that supercoiling can modify protein expression, and the necessity to provide supercoiling-independent biological parts for future rational designs. Additionally, I implemented a model of supercoiling in Matlab and integrated a novel model of the insulator part. A secondary objective of this project was testing the designs in a new transcription-translation (TX-TL) system, where no expression of the downstream gene (*rff*) was detected.

# Contents

---

<b>1</b>	<b>INTRODUCTION</b>	<b>3</b>
<b>2</b>	<b>BACKGROUND</b>	<b>4</b>
2.1	SYNTHETIC BIOLOGY	4
2.2	TRANSCRIPTION-TRANSLATION SYSTEMS	4
2.3	SUPERCOILING	5
2.4	MOTIVATION FOR THIS PROJECT	6
<b>3</b>	<b>DESIGN</b>	<b>7</b>
<b>4</b>	<b>MATERIALS AND METHODS</b>	<b>9</b>
4.1	PLASMID CONSTRUCTION	9
4.2	CULTURE CONDITION	9
4.3	MEASUREMENTS OF PROTEIN EXPRESSION	9
4.3.1	<i>Culture</i>	9
4.3.2	<i>TX-TL</i>	10
4.3.3	<i>Flow cytometer</i>	10
4.4	PROTOCOLS	10
4.4.1	<i>TX-TL</i>	10
4.4.2	<i>Polymerase Chain Reaction (PCR)</i>	10
4.4.3	<i>PCR colony</i>	11
4.4.4	<i>Preparing chemically competent cells</i>	12
4.4.5	<i>Cell transformation</i>	12
4.4.6	<i>Sequencing</i>	12
4.4.7	<i>Gel purification</i>	12
4.4.8	<i>Plasmid extraction (Miniprep)</i>	13
4.4.9	<i>Gibson assembly</i>	13
4.5	DATA ANALYSIS	15
<b>5</b>	<b>MODELLING</b>	<b>16</b>
5.1	EXISTING MODELS	16
5.2	IMPLEMENTATION	17
5.3	SIMULINK	18
5.4	THE INSULATOR	19
<b>6</b>	<b>RESULTS</b>	<b>21</b>
6.1	GENERATING SUPERCOILING	21
6.2	DETECTING SUPERCOILING	22
6.3	EFFECT ON CONSTITUTIVE PROMOTER	23
6.4	THE INSULATOR	24
6.5	TX-TL	24
<b>7</b>	<b>DISCUSSION</b>	<b>25</b>
<b>8</b>	<b>CONCLUSION</b>	<b>27</b>
<b>9</b>	<b>FUTURE WORK</b>	<b>28</b>

9.1	DISTANCE .....	28
9.2	THE IMPROVED INSULATOR .....	28
9.3	SUPERCOILING MAP .....	28
<b>10</b>	<b>ACKNOWLEDGEMENTS .....</b>	<b>30</b>
<b>11</b>	<b>REFERENCES .....</b>	<b>31</b>
<b>12</b>	<b>APPENDIX .....</b>	<b>33</b>
12.1	LIST OF PRIMERS .....	33
12.2	PROGRAM CODE .....	33

# 1 Introduction

---

Precise control of genetic circuits is of vital importance in synthetic biology. In order for the circuits to be practical they must be able to operate under a variety of different circumstances. Genetic transcription events modify the topology of the neighbouring DNA. These topological changes can then lead to different levels of gene expression. One topological effect that has been reported in literature is DNA supercoiling.

The aim of this project is to quantify the effects of DNA supercoiling and investigate whether it can be regulated by inserting a specific sequence upstream of the genetic circuit. This sequence has been suggested to function as a supercoiling insulator. I constructed three circuits that are designed to test this. Section 3 details the design process including justification for the parts and plasmids that were used.

In order to understand the different processes and components of supercoiling interaction, I implemented a mathematical model in Matlab. This is a model of the compositional context of the system, including supercoiling effects. In addition, I modelled the insulator element and integrated it into the existing model. Section 5 contains this work.

The parts were tested *in vitro* - in a TX-TL system and *in vivo*. Experimental materials and methods are explained in section 4, with the results presented in section 6. The results from culture showed that gene transcription is influenced by the intensity of upstream transcription events. Tests in TX-TL were inconclusive as no protein expression could be observed. The limitations of the report as well as suggestions for improvements are discussed in sections 7 to 9.

## 2 Background

### 2.1 Synthetic biology

The aim of synthetic biology is the creation and assembly of biological systems that behave in a way not found in nature. This is done by modifying the genetic composition of living organisms. Sequences of DNA are inserted or removed from natural genomes, resulting in modified gene expression. In recent years these sequences have started to become increasingly standardised. Therefore, genetic circuits, analogous to electrical circuits, are now being designed using standard parts and components.

With the aid of mathematical and computer modelling these genetic circuits can be simulated before being realised *in vivo*. This helps reduce development time and can improve the efficiency of the circuits. The predictability and behaviour of every part is important for them to be modelled accurately.

### 2.2 Transcription-translation systems

This subsection is adapted from: Kolbeinsson, Arinbjörn. *Cell-free and supercoiling – Interim report*. 2015.

In 1961 Nirenberg and Matthaei created the first cell-free extract capable of protein synthesis. By adding particular nucleobases to cell extract, they induced the synthesis of specific amino acids. Although this experiment is generally known for “cracking the genetic code” the method they used carries great potential<sup>1</sup>.

Cell-free systems can be created by mixing crude cell extract, template mRNA and amino acids. Together with a supply of energy (composed of HEPES, ATP, GTP, CTP, UTP, tRNA, CoA, NAD, cAMP, folic Acid, Spermidine and 3-PGA) this solution can synthesise protein from the given mRNA. The cell extract includes the translation machinery required for protein translation and can operate outside a live cell<sup>2</sup>. More advanced systems have been developed which transcribe DNA into mRNA before translating it into protein<sup>20</sup>.

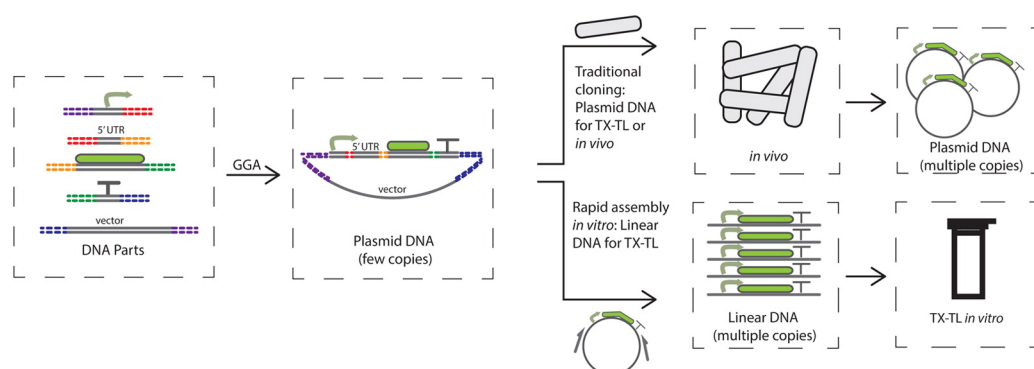


**Figure 1.** A comparison of *in vivo* and TX-TL methodology. Cloning and transformation is required for *in vivo* experiments and can take days to complete. This is not needed for TX-TL experiments and hence total implementation time is reduced. Figure adapted from Sun et al., 2014<sup>20</sup>.

Recently, cell-free synthetic biology has emerged as a versatile prototyping environment (Figure 1). Testing gene circuits *in vitro* has a number of advantages over traditional *in vivo* approaches. These include reduced system complexity and shorter design cycle times. Two of the most time consuming steps of *in vivo* experiments are cloning and cell-transformation, which are not required for transcription-translation (TX-TL) systems and therefore the cycle time is greatly reduced. Endogenous DNA and mRNA are

removed during the extract preparation to isolate the circuit from potential interference by the cellular host<sup>3</sup>.

The falling prices of TX-TL systems have made them an attractive choice for high yield production of materials. Compared with *in vivo* methods, these systems are more efficient in conditions that are not optimal for bacterial growth such as toxic, high temperature or low pH environments. An example of the practicality of such systems is human protein manufacture<sup>4</sup>. These have potential medical applications. Furthermore, TX-TL has been used to produce hydrogen from starch and water in a spontaneous process<sup>5</sup>. Hydrogen is seen as a key future energy source.

TX-TL can also be used to study *in vivo* processes. The TX-TL environment is far simpler than that of the cell, which makes observing specific characteristics of cell activity easier<sup>3</sup>. One feature of interest is the resource competition between cell growth and protein expression. This can be accomplished *in vitro* by comparing the burden on the system caused by synthetic devices and cell metabolism as growth cannot be directly measured in a TX-TL solution.

TX-TL systems are not without their limitations. Reactions and protein production can usually be sustained for only 4 to 8 hours<sup>3</sup>. On top of that, some systems have been shown to be independent of resources for only the first half of the reaction time. Extended gene expression times are required for larger and more complex gene circuits. Other limitations include amino acid degradation, build-up of waste and pH change, which affect gene expression<sup>6</sup>.

### 2.3 Supercoiling

DNA supercoiling is the overwinding or underwinding of the DNA double helix. A relaxed B-DNA helix will coil once every 10.5 base pairs (bp). Deviations from this configuration will cause the whole molecule to twist back on itself and form a coil. There are two basic types of supercoil conformations, positive ( $>10.5$  turns per bp) and negative ( $<10.5$  turns per bp). Supercoiling can affect the transcription rate of genes. In most cases when the DNA is overwound, more energy is required to separate the strands, leading to decreased transcription efficiency<sup>19</sup>. Supercoiling occurs naturally during transcription, replication, repair and other DNA operations<sup>8,18</sup>.

During DNA synthesis the RNA polymerase (RNAP) requires an unwound region of the DNA strand. As a consequence of this requirement, DNA in the surrounding region will deform with positive supercoils ahead of the region and negative supercoils behind<sup>8,16</sup>. Further supercoiling occurs as the RNAP tracks along the strand<sup>17</sup>. Although the DNA is not anchored and is able to rotate freely, natural bends and kinks in the double strand increase drag and impede rotation of the entire backbone; resulting in localised supercoiling<sup>7</sup>. The cell regulates the level of supercoiling with specialised equipment that have two modes of operation. The types of enzymes that carry out these operations are known as topoisomerases<sup>8</sup>.

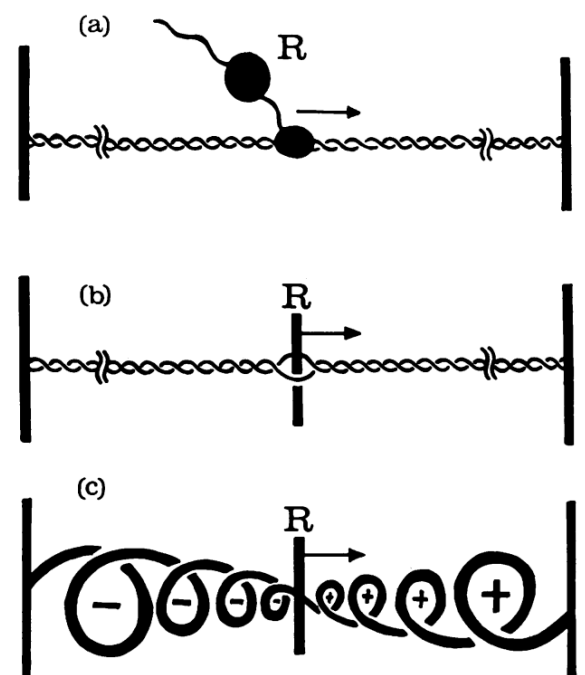


**Figure 2.** An illustration of the transcription complex (labelled R) operating on DNA. As it moves down the strand, supercoils will form on both sides. The ends can be considered fixed due the high drag of distant DNA. Figure is adapted from Liu et al., 1987<sup>17</sup>.

Two key topoisomerases are topoisomerase I and II, which work in opposite. Topoisomerase II is commonly known DNA gyrase. Gyrase adds negative supercoils to DNA and is homeostatically regulated by the genes *gyrA* and *gyrB*. Conformal changes induced by supercoiling affect the gene expression leading to increased gyrase concentration. The gyrase then reduces the level of supercoiling and the expression of gyrase is reduced. The mechanism of the gyrase action is well understood. The enzyme relieves positive supercoiling by cleaving both strands of the double helix and allowing an intact strand to pass through<sup>8</sup>.

The activity of the promoter upstream of *gyrA*, named  $P_{gyrA}$ , is regulated by supercoiling level<sup>9</sup>. For this reason, it has been used to detect local TI supercoiling<sup>10</sup>. This was accomplished by placing a  $P_{gyrA}$ -*lacZ* complex downstream of an inducible transcription unit. The idea was that the positive supercoils from the upstream unit would propagate downstream and induce the  $P_{gyrA}$  promoter. The two units were separated by a terminator<sup>10,18</sup>.

In that study, increased  $P_{BAD}$  activity raised *LacZ* expression, indicating that positive supercoiling had diffused across the terminator. This was demonstrated with two control experiments. First, when the *gyrA* promoter was not present, *LacZ* was not expressed. This indicates that the terminator was functional and had stopped the reading. For the second control, both the inducible transcription unit and the terminator were removed. In this configuration *LacZ* was expressed at a relatively constant rate. These results suggest that supercoiling effects diffuse at least several kilobases (kb) away from the transcription site<sup>10,18</sup>.

Also tested in that study is a sequence which might function as a supercoiling diffusion inhibitor. This sequence is a DNA gyrase binding and cleavage site. By placing this sequence in front of the  $P_{gyrA}$ -*lacZ* unit the authors measured the effect of the binding site. They found that with the insulator sequence present, the activity of  $P_{gyrA}$  was decreased. The authors hypothesised that this was due to gyrase binding to the insulator site enabling them to efficiently add negative supercoils<sup>18</sup>.

Supercoiling has been proposed as a second messenger<sup>11</sup>. The study found 306 genes in the genome of *E. coli* MG1655 that were affected by changes in supercoiling levels. The authors argue that the cells use supercoiling levels to detect changes in environmental growth conditions, including  $O_2$  levels and ionic strength.

## 2.4 Motivation for this project

Supercoiling can affect synthetic biological systems in two main ways. Most importantly, transcription of genes can cause DNA in the surrounding area to become supercoiled. If a sensitive circuit or part is within the range of these deformations, it can have undesirable consequences. In extreme cases a circuit might become unstable and depending on the role of that circuit, for example a drug delivery system, could be catastrophic. Secondly, supercoils generated from the synthetic circuit can affect normal regulatory networks in the cell. This could have various consequences on cell growth and regulation, depending on the circuit and its location in the genome.

In this project I want to quantify the effects TI supercoiling has on downstream transcription events. Furthermore, I want investigate ways to reduce these effects.

### 3 Design

To investigate the effects of supercoiling on downstream transcription, I planned on building a construct that both responds to changes in and produces supercoiling. To regulate TI supercoiling I selected the  $P_{BAD}$  promoter, which is inducible with arabinose. Supercoiled DNA using this promoter has been shown to diffuse at least 5 kb from the transcription site using manageable concentrations of arabinose<sup>10</sup>. Using the  $P_{BAD}$  promoter to drive a green fluorescent protein (*gfp*) gene was preferred, as GFP expression can be detected by an automated plate reader.

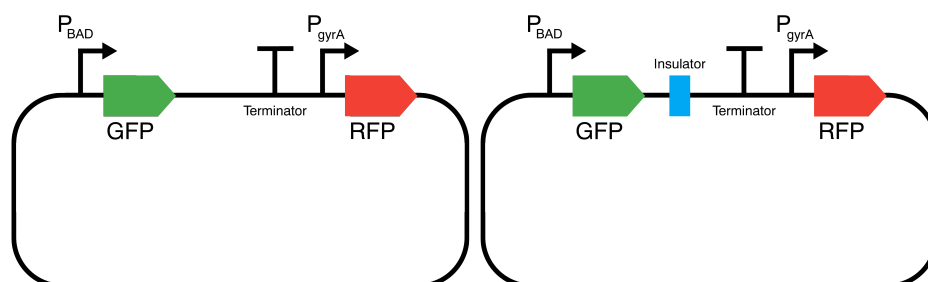


**Figure 3.** Schematic representation of plasmids EAK-NG (left) and EAK-IG (right). The difference between the two constructs is the addition of an insulator element (blue box) to EAK-IG. Supercoils should propagate away from the  $P_{BAD}$  unit and affect the induction of  $P_{gyrA}$ . The insulator should reduce these supercoils to a certain degree. Both plasmids carry ampicillin resistance.

$P_{gyrA}$ , the promoter of the gyrase gene *gyrA*, is involved in homeostatic control of supercoiling. This promoter had previously been used to investigate supercoiling<sup>9,10</sup>. As DNA becomes increasingly supercoiled at the  $P_{gyrA}$  region the promoter will become increasingly activated. However, at very high levels of supercoiling, the efficiency of transcription will drop by more than what the promoter can induce. Hence, I expect to observe a peak of  $P_{gyrA}$  activity at some arabinose concentration. I decided to use red fluorescent protein (*rfp*) as a measure of  $P_{gyrA}$  activity for the same reason as *gfp*. These two aforementioned complexes, the supercoiling generator and detector, would need to be separated by a strong terminator to ensure that transcription would not continue from the upstream unit to the other.

A plasmid that contains  $P_{BAD}$ -*gfp*-Ter-*rfp*, had already been constructed and tested<sup>12</sup>. This plasmid (pGR-L3S2P21) could be used as a backbone for my constructs. With the insertion of  $P_{gyrA}$  ahead of the *rfp* gene, a circuit matching my specification could be assembled. The only major drawback with using the pGR-L3S2P21 plasmid was the presence of BsaI sites. This meant that Golden Gate assembly is difficult to use. However, this disadvantage is slightly offset by that fact that this setup requires only one Gibson assembly to join the  $P_{gyrA}$  to the backbone. A third reason for selecting the pGR-L3S2P21 was the strong synthetic terminator (L3S2P21) separating the two complexes. The plasmid has ampicillin resistance and has been tested in *E. coli* DH10B cells, Figure 3.

Next, I wanted to know if supercoiling had an effect on the transcription rate of a conventional constitutive promoter. This promoter should not have any specific relationship with the supercoiling level, but rather act as a proxy for any general promoter that I, or anyone else, would use. I decided to use a weak promoter to ensure I would observe the complete range of effects. A promoter that is too strong could saturate at low supercoiling levels, if supercoiling has an effect. The promoter must also be independent of the arabinose concentration used to induce the  $P_{BAD}$  promoter. Given these specifications I found the J23107 to be a suitable solution. This promoter exhibits no regulated elements and is an intermediate strength member of the constitutive promoter J23119 family.

Finally, I wanted to see if a specific sequence could be inserted between the two complexes that would block or insulate supercoiling. The sequence I wanted to test has been suggested as a likely candidate for topological insulation<sup>10</sup>. In that study the authors inserted the insulator element between the upstream gene and the terminator. I decided to use this configuration in the hope of replicating the results. An interesting modification would be to place the insulator in front of the promoter. This paves the way for an ‘isolated promoter’ biobrick. Two new constructs would have to be made; the insulator combined with both P<sub>gyrA</sub> and the constitutive promoter, separately. Figure 4 visualises the former of those constructs. The insulator sequence is a type 2 bacterial interspersed mosaic element (BIME), or BIME-2 *nrdAB*, that has been associated with gyrase binding and cleavage<sup>21</sup>.

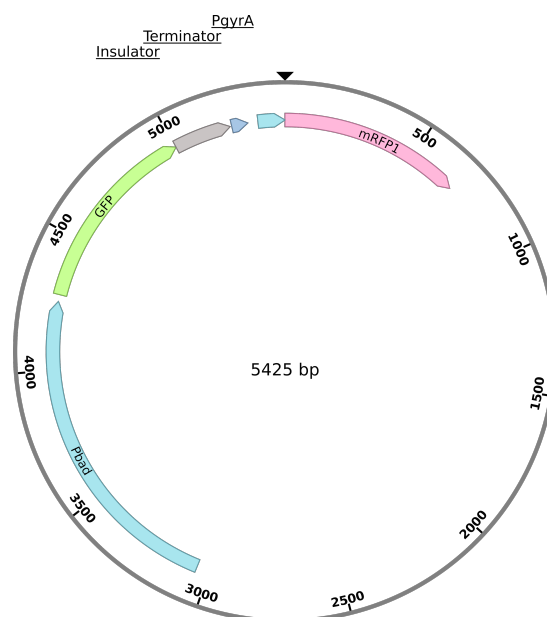


**Figure 4.** Visualisation of EAK-IG. The P<sub>gyrA</sub> promoter and insulator have been inserted into the pGR-L3S2P21 plasmid.

**Table 1.** Plasmids for this project. The insulator element (INS) is a BIME-2 *nrdAB* sequence. The terminator (Ter) is L3S2P21.

Name	Description	Reference
pGR-L3S2P21	P <sub>BAD</sub> - <i>gfp</i> -Ter- <i>rff</i>	Chen et al., 2013 <sup>12</sup>
EAK-NG	P <sub>BAD</sub> - <i>gfp</i> -Ter-P <sub>gyrA</sub> - <i>rff</i>	This work
EAK-IG	P <sub>BAD</sub> - <i>gfp</i> -INS -Ter -P <sub>gyrA</sub> - <i>rff</i>	This work
EAK-NJ	P <sub>BAD</sub> - <i>gfp</i> -Ter-P <sub>J23107</sub> - <i>rff</i>	This work
EAK-IJ*	P <sub>BAD</sub> - <i>gfp</i> -INS -Ter -P <sub>J23107</sub> - <i>rff</i>	This work

The comparison of supercoiling in different chassis is outside the scope of this project. I decided to use *E. coli* primarily because the backbone and genetic parts I selected have been tested in *E. coli*. Additionally, it is one of the most common synthetic biology chassis and is well studied, which could lead to more rapid troubleshooting. I chose strain DH10B for similar reasons, and the insulator element I was implementing had been tested in DH5 $\alpha$ <sup>10</sup>.

\* This plasmid was designed but not successfully constructed.

## 4 Materials and methods

---

### 4.1 Plasmid construction

The pGR-L3S2P21 plasmid, to be used as a backbone, from Addgene.  $P_{gyrA}$  was isolated from genomic *E. coli* DNA. The plasmid backbone was PCR-amplified using the pGR-L3S2P21\_part1 FWD and pGR-L3S2P21\_part1 REV primers, see Table 9. Similarly,  $P_{gyrA}$  was PCR-amplified using  $P_{gyrA}$  FWD and  $P_{gyrA}$  REV. The  $P_{gyrA}$  fragment was then isolated using gel purification. Using the Gibson assembly method† the  $P_{gyrA}$  fragment was inserted into the plasmid.

The J23107 constitutive promoter was ordered from Registry of Standard Biological Parts‡. It was PCR amplified using OB\_J23107 FWD and OB\_J23107 REV. The promoter was cloned into the pGR-L3S2P21 plasmid using Gibson assembly.

The insulator element was isolated from genomic DNA. It was PCR-amplified using the Insulator FWD and Insulator REV oligos. The fragment was isolated using gel purification. Using the Gibson assembly method, the insulator fragment was inserted into the plasmid containing  $P_{gyrA}$ .

### 4.2 Culture condition

The four constructed plasmids and the unaltered pGR-L3S2P21 plasmid were transformed into chemically competent *E. coli* DH10B cells prepared earlier and let grow overnight on ampicillin agar plates (100 µg/ml). Five colonies were selected and colony PCR, in addition to gel electrophoresis, were used to identify cells containing the correct clones based on plasmid size. These colonies were then grown in an overnight culture of 5 ml LB media with 5 µl ampicillin (100 mg/ml). The DNA from these cells was then extracted and sent for sequencing to check the result of cloning. After confirming the plasmid had been successfully constructed§ the DNA was transformed into chemically competent *E. coli* DH10B and grown at 37°C overnight in a shaker (ThermoScientific MaxQ 6000) at 225 rpm.

### 4.3 Measurements of protein expression

#### 4.3.1 Culture

5 µl of overnight culture was pipetted into 60 centre wells of a 96-well plate (Corning Costar) containing 95 µl of LB media. Different plasmids arranged down the columns and arabinose concentration varied along the rows. The edge wells were not used due condensation forming under certain circumstances near the edges of the plate cover. The plate was covered the plate with a breathable film and placed in a plate reader (Bio-Tek Synergy HT, USA), which had been preheated to 37°C. Green fluorescence was measured at excitation 485 nm, emission 528 nm with a gain of 60. Red fluorescence was measured at excitation 590 nm, emission 645 nm with a gain of 60. The plate reader was programmed to perform the following protocol every 5 minutes for 24 hours:

1. Shake for 2 minutes
2. Read green fluorescence
3. Read red fluorescence

---

†Golden Gate assembly was more difficult to use than Gibson assembly due to the presence of BsaI sites in the pGR-L3S2P21 plasmid.

‡ [http://parts.igem.org/Main\\_Page](http://parts.igem.org/Main_Page)

§ The construction of the EAK-IJ plasmid was not successful.

After the plate readings had completed, 50  $\mu$ l of 50% glycerol was pipetted into each well, the plate covered with a breathable film and stored at  $-80^{\circ}\text{C}$ .

#### 4.3.2 TX-TL

1.2  $\mu$ l of 10 times diluted DNA was pipetted into a 384-well microplate. Adjacent wells were not used as they might interfere with each other. I then pipetted 1.5  $\mu$ l of varying concentrations of arabinose solution into the wells containing DNA. 7.88  $\mu$ l of the TX-TL master mix was rapidly pipetted into the same wells. I then covered the plate with film and centrifuged the plate for 2 min at 200 rpm and  $4^{\circ}\text{C}$  to ensure all solution had collected at the bottom of each well. Immediately after centrifuging the plate was placed in a plate reader (Synergy HT, BioTek, USA) at  $29^{\circ}\text{C}$ . Green fluorescence was measured at excitation 495 nm, emission 528 nm with a gain of 60. Red fluorescence was measured at excitation 590 nm, emission 645 nm with a gain of 60. The plate reader was programmed to perform the following protocol every 5 minutes for 21 hours and 40 minutes:

4. Slow shake for 2 minutes
5. Read green fluorescence at normal speed
6. Read red fluorescence at normal speed

#### 4.3.3 Flow cytometer

A clean 96-well plate (Corning Costar) was prepared by pipetting 200  $\mu$ l of sterile water into each well. The culture plate that had previously been tested in the plate reader four days earlier, and stored at  $-80^{\circ}\text{C}$  since, was removed from the freezer. Using a multichannel pipette, I pressed lightly on the frozen cultures with sterile tips. I then submerged the tip into the corresponding well of the new 96-well plate. I repeated this for all the wells containing culture.

I also prepared two calibration samples. One containing WT DH10B culture and the other containing plasmid EAK-NG in 25  $\mu\text{M}$  arabinose. The flow cytometer (FACScan, Becton Dickinson, USA) was set up and gated using these samples.

### 4.4 Protocols

#### 4.4.1 TX-TL

A TX-TL cell-free system was constructed as described in Sun et al., 2013<sup>13</sup> using Rosetta BL21. Crude cell extract was prepared by bead beating pelleted cells and filtering the extract using a special apparatus. Additionally, an energy solution (containing HEPES, Nucleotides Mix, tRNA, CoA, NAD, cAMP, folic acid, spermidine and 3-PGA) and buffer (Mg-glutamate, K-glutamate and DTT) were made. An amino acid solution (2 mM Mg-glutamate, 38.2 mM K-glutamate, 3mM of each amino acids 2.1  $\mu$ l of energy solution, 1mM DTT and 4% PEG-8000) was made and flash frozen to store at  $-80^{\circ}\text{C}$ . This task was led by Dr Olivier Borkowski.

#### 4.4.2 Polymerase Chain Reaction (PCR)

The following reagents (Table 2) were mixed in a 1.5  $\mu$ l PCR tube. All reagents (except for DMSO) and DNA are kept on ice during this period. The PCR tube is then briefly vortexed and centrifuged, to ensure thorough mixing, and is placed in a thermal cycler (Eppendorf Mastercycler gradient, Germany) and cycled at the following routine.

Thermocycling program

1.  $98^{\circ}\text{C}$  for 30 s
2.  $98^{\circ}\text{C}$  for 30 s
3.  $55^{\circ}\text{C}$  for 30 s
4.  $72^{\circ}\text{C}$  for 30 s per kb

5. Repeat previous three steps 30 times
6. 72°C for 10 min
7. Hold at 10°C

The tube is then stored at 4°C.

**Table 2.** Materials and amounts needed for a single PCR reaction.

Reagent	Amount
Oligo 1	0.5 µl
Oligo 2	0.5 µl
DNA	0.5 µl
5X Phusion HF Buffer	10 µl
10 mM dNTP	0.5 µl
DMSO	1.5 µl
Phusion DNA Polymerase	0.2 µl
Nuclease free water	36.3 µl

#### 4.4.3 PCR colony

The reagents detailed below (Table 3) are mixed in a PCR tube. A sterile pipette and tip are used to gently touch the colony of interest and then dipped into the reaction mix. The tube is then placed in a thermal cycler.

**Table 3.** Materials and amounts needed for a single colony PCR reaction.

Reagent	Amount
Oligo 1	0.5 µl
Oligo 2	0.5 µl
Colony	trace
5X Phusion HF Buffer	10 µl
10 mM dNTP	0.5 µl
DMSO	1.5 µl
Phusion DNA Polymerase	0.2 µl
Nuclease free water	36.8 µl

#### Thermocycling program

1. 98°C for 6 min 30 s
2. 98°C for 30 s
3. 55°C for 30 s
4. 72°C for 30 s per kb
5. Repeat previous three steps 35 times
6. 72°C for 10 min
7. Hold at 10°C

#### 4.4.4 Preparing chemically competent cells

Protocol is adapted from Chung et al., 1993<sup>14</sup>

1. A 5 ml overnight culture of cells is grown in LB media. In the morning, this is diluted back into 50 ml of fresh LB media in a 200 ml conical flask
2. The culture was grown to an OD<sub>600</sub> of 0.5
3. Put new Eppendorf tubes on ice now so that they are cold when cells are aliquotted into them later. If your culture is X ml, you will need X tubes. At this point you should also make sure that your TSS is being chilled
4. Cultures are split into two 50 ml falcon tubes and incubated on ice for 10 min
5. Falcon tubes were centrifuged for 10 minutes at 3,000 rpm and 4°C
6. Supernatant is poured off
7. Pelleted cells are resuspended in 5 ml chilled TSS buffer
8. Add 100 µl aliquots to Eppendorf tubes on dry ice and store at -80°C in freezer (New Brunswick Scientific Innova U535, USA)

**Table 4.** Materials and amounts needed for TSS buffer.

Reagent	Amount
PEG 8000	5 g
MgCl <sub>2</sub>	1.2 ml
DMSO	2.5 ml
LB media	Complete to 50 ml

#### 4.4.5 Cell transformation

Protocol is adapted from Chung et al., 1993<sup>14</sup>

1. Cells previously prepared with TSS buffer are thawed on ice
2. 1 µl of DNA is added to 100 µl of cells
3. Kept on ice for 30 min
4. Incubated in water bath at 42°C for 30 s
5. Placed on ice for 2 min
6. 1 ml of LB added to every tube
7. Incubated for 1 h at 37°C on shaker at 225 rpm
8. Cells were spread onto a plate made with appropriate antibiotic
9. Grown in an incubator overnight at 37°C

#### 4.4.6 Sequencing

10 µl samples (concentration between 50 and 100 ng/µl) were sent for sequencing to SourceBioscience, UK for Sanger sequencing services.

#### 4.4.7 Gel purification

Protocol is adapted from QIAGEN QIAquick miniprep handbook

1. DNA bands for extraction were identified using a UV transilluminator (Bio-Rad Laboratories UV Transilluminator 2000, USA)
2. Using a razor blade, the desired piece from the gel is removed and placed in a 1.5 ml Eppendorf tube
3. Three gel volumes of Buffer QG was added to the tube
4. Incubated at 45°C for 10 min or until gel is fully dissolved
5. Vortexed briefly
6. Sample is transferred to a QIAquick column in a collection tube

7. Centrifuged at 13,400 rpm for 60 s and discarded flow-through
8. Pipetted 500  $\mu$ l of buffer QG to column
9. Centrifuged at 13,400 rpm for 60 s and discard flow-through
10. Pipetted 750  $\mu$ l of buffer PE to column
11. Centrifuged at 13,400 rpm for 60 s and discard flow-through
12. Centrifuged again to remove any residual buffer
13. Placed column in a 1.5 ml Eppendorf tube
14. Added 30  $\mu$ l of elution buffer EB to centre of column
15. The tube is allowed to stand for 60 s
16. Then centrifuged at 13,400 for 60 s
17. DNA that collected in tube is stored at -20°C

#### 4.4.8 Plasmid extraction (Miniprep)

Protocol is adapted from the QIAGEN QIAquick miniprep handbook

1. 10 ml cell culture tube was centrifuged at 4,000 rpm for 5 min
2. Supernatant was poured off
3. Pelleted bacterial cells were resuspended in 250  $\mu$ l Buffer P1 and transferred to a 1.5 ml Eppendorf tube
4. 250  $\mu$ l of Buffer P2 was added and the tube gently inverted 5 times to mix
5. 350  $\mu$ l of Buffer N3 was added and the tube immediately inverted 5 times
6. Tube was then centrifuged for 10 min at 13,400 rpm in a table-top microcentrifuge (Eppendorf minispin, Germany)
7. Supernatant was poured into a clean QIAprep spin column, making sure none of the pellet is displaced
8. Centrifuge for 60 s at 13,400 rpm, discard the flow-through
9. QIAprep spin column was washed by adding 0.75 ml of buffer PE, centrifuging for 60 s and then discarding the flow-through
10. Previous step was repeated
11. Spin column was centrifuged for an additional 60 s to remove residual buffer
12. QIAprep column was placed in a clean 1.5 ml Eppendorf tube. 50  $\mu$ l of sterile water at room temperature was added to the centre of the QIAprep spin column, let to stand for 1 min, and centrifuge for 1 min
13. DNA concentrations was checked by placing 1  $\mu$ l of solution in a nanosizer (Thermo Scientific NanoDrop 1000 Spectrophotometer)

#### 4.4.9 Gibson assembly

Protocol is adapted from Gibson et al, 2009<sup>15</sup>. Tables 5 to 8 detail the reagents needed and their amounts.

**Table 5. Materials and amounts for a 5X isothermal reaction mix.**

Reagent	Amount
Tris-Hcl (pH 7.5)	3 ml 1 M
MgCl <sub>2</sub>	300 $\mu$ L 1 M
dGTP	60 $\mu$ L 100 mM
100 mM dATP	60 $\mu$ L
100 mM dTTP	60 $\mu$ L
100 mM dCTP	60 $\mu$ L
1 M DTT	300 $\mu$ L
PEG-8000	1.5 g

100 mM NAD	300 $\mu$ L
ddH <sub>2</sub> O	Fill to 6 ml

**Table 6.** Materials and amounts for the assembly master mix.

Reagent	Amount
5X Isothermal Master Mix	320 $\mu$ L
T5 exonuclease	0.64 $\mu$ L 10 U/ $\mu$ L
Phusion DNA Pol	20 $\mu$ L 2 U/ $\mu$ L
Taq DNA Ligase	0.16 $\mu$ L 40 U/ $\mu$ L
ddH <sub>2</sub> O	860 $\mu$ L

**Table 7.** Materials and amounts for 5X isothermal reaction buffer.

Reagent	Amount
25% PEG-8000	0.75 g
500 mM Tris-HCl pH 7.5	1500 $\mu$ l
50 mM MgCl <sub>2</sub>	75 $\mu$ l
50 mM DTT	150 $\mu$ l
5 mM NAD	300 $\mu$ l
1 mM each of the four dNTPs	30 $\mu$ l each

**Table 8.** Materials and amounts for 1.33X Gibson master mix

Reagent	Amount
Taq ligase (40u/ $\mu$ l)	50 $\mu$ l
5x isothermal buffer	100 $\mu$ l
T5 exonuclease (1u/ $\mu$ l)	2 $\mu$ l
Phusion polymerase	6.25 $\mu$ l

(2u/ $\mu$ l)		216.75 $\mu$ l
Nuclease-free water		

1. Thaw a 15  $\mu$ l 1.33X Gibson master mixture aliquot and keep on ice until ready to be used
2. Add 5  $\mu$ l of DNA to be assembled to the Gibson master mix. The DNA should be in equimolar amounts  
Use 10-100 ng of each  $\sim$ 6 kb DNA fragment. For larger DNA segments, increasingly proportionate amounts of DNA should be added (e.g. 250 ng of each 150 kb DNA segment)
3. Incubate at 50  $^{\circ}$ C for 60 min
4. Keep at 4 $^{\circ}$ C

#### 4.5 Data analysis

The fluorescence data are time synchronised to the onset of the exponential-growth phase of each sample based on  $OD_{600}$  curves. The autofluorescence of wild type DH10B cells is then subtracted from the raw data. To correct for differences in cell numbers and density the fluorescence values for each well is divided by the respective  $OD_{600}$  values. Due to the division the uncertainty need to be properly accounted for. To do this I add the normalised errors for both fluorescence and  $OD_{600}$  ( $FL_{\text{error}}/FL + OD_{\text{error}}/OD$ ), and then combine with the normalised fluorescence.

Shaded error line plots were graphed using *boundedline.m*, a Matlab script available on Matlab Central.<sup>22</sup> Bar plot was graphed using *batwitherr* available on Matlab Central.<sup>23</sup>

## 5 Modelling

---

### 5.1 Existing models

Recently, a model was developed to describe how the spatial arrangement of parts affect transcription in an *E. coli* based TX-TL system<sup>16</sup>. This was done by modelling the impact of supercoiling, R-loop formation and terminator leakage. The model builds on Liu and Wang's pioneering twin-supercoiled domain model<sup>17</sup>. Their mathematical model describes the mechanics of the double helix as the RNAP proceeds along it. DNA behind the RNAP will become negatively supercoiled and DNA in front of the RNAP will become positively supercoiled.

The authors of this new TX-TL model study transcription in three different configurations. Firstly, convergent, where the genes are transcribed towards each other, secondly divergent, where the genes are transcribed away from each other and finally, in tandem. Since my constructs are all organized in a tandem orientation, where genes are oriented in the same direction, I will focus on this configuration.

The supercoiling is modelled at four locations in the genome; at the two promoters and at the two transcription sites.<sup>16</sup> The authors argue that supercoiling affects the efficiency of the transcription elongation complex; with any perturbations from the intrinsic supercoiling level leading to reduced transcription rates. They model the change in supercoiling at the downstream promoter as a combination of four terms. The first term is the effect of the upstream promoter on the downstream promoter:

$$k_{cat}(\sigma_{p,U})EC_U \frac{TL_U}{2(PL_d + n_S)}$$

It is a function of the catalytic rate of the system  $k_{cat}$ , which is a function of the supercoiling density at the upstream promoter  $\sigma_{p,U}$ .<sup>\*\*</sup> This is multiplied by  $EC_U$ , the concentration of transcription complexes that are working on transcribing the upstream gene. Finally, the distances have to be taken into account. Supercoiling decreases as the distance from the upstream transcription site increases. This is governed by the upstream transcription length  $TL_U$ , downstream promoter length  $PL_d$ , and the intergenic region distance  $n_S$ . The second term is the effect of the downstream promoter on itself:

$$-kf(\sigma_{p,D})p_U R$$

This term is a function of the promoter strength  $p_U$ , transcription initiation rate  $k_f$  and the concentration of free ribosomes  $R$ . The third term describes the effect of the downstream transcription on the downstream promoter. It is similar to the first one with the only major difference being the sign. The negative sign arises from the fact that negative supercoils propagate upstream from the transcription site.

$$-k_{cat}(\sigma_{t,d})EC_D \frac{TL_D}{2(PL_D + n_S)}$$

---

<sup>\*\*</sup>  $\sigma$  is a measure of supercoiling density with respect to a relaxed DNA molecule. A region of DNA with  $\sigma = 1$  has one more supercoiling turn compared to a relaxed DNA region.

The final term models the homeostatic regulation by topoisomerase I and gyrase within the cell:

$$\frac{h_0}{PL_D}(\tau 1_{\sigma < \sigma_0} - \gamma 1_{\sigma > \sigma_0})$$

Topoisomerase I and gyrase attempt to keep the supercoiling level at  $\sigma_0 = -0.65$ . Depending on the current supercoiling, either one of the enzymes will be active. This is represented with the Boolean  $1_x$  function. If  $x$  is true it takes a value of 1, and 0 otherwise.  $\tau$  and  $\gamma$  are the rates of supercoiling modification by topo I and gyrase, respectively.  $h_0$  is the number of base pairs per helical DNA turn and  $PL_d$  is the downstream promoter length.

The first three terms are scaled by  $\Omega$ , which is the reaction volume divided by the volume of a single cell. This is to compensate for the use of *in vivo* parameters. If TX-TL parameters are used this factor can be omitted. Bringing all this together yields the complete equation:

$$\begin{aligned} \sigma_{p,D} = \frac{\Omega}{2} & \left( k_{cat}(\sigma_{p,U}) EC_U \frac{TL_U}{2(PL_D + n_S)} - kf(\sigma_{p,D}) p_{UR} - k_{cat}(\sigma_{t,d}) EC_D \frac{TL_D}{2(PL_D + n_S)} \right) \\ & + \frac{h_0}{PL_D} (\tau 1_{\sigma < \sigma_0} - \gamma 1_{\sigma > \sigma_0}) \end{aligned}$$

The complete set of equations and further explanations can be found in the paper by Yeung et al., 2014<sup>16</sup>.

## 5.2 Implementation

I implemented the whole model directly in Matlab using the Euler integration method. The Euler method has a certain degree of error, but the system parameters have not been tuned to accurately represent experimental results. Given this factor I assume the integration error would be negligible when compared to the overall system. However, I did try to minimise the errors wherever possible and one way of achieving that is by reducing the step size. I chose a step size of 0.036 s and 400,000 iterations, giving a total simulation time of 14,000 s, or four hours.

When testing the model in Matlab using the parameters described in the original paper<sup>16</sup>, the output was not as expected. The system displayed unstable oscillations that eventually crashed the simulation before all 400,000 iterations could be completed. After closely investigating the dynamics of the model, I made a few modifications to the code:

1. The number of transcription units transcribing the two genes at  $t = 0$  was set to 0.
2. The units of  $\beta$  were changed from  $s^{-1}$  to  $nM s^{-1}$ , to reflect the units of  $\zeta$ .
3. The parameter  $k_w$  was set to  $10^{-9}$ , as I was simulating the system in M, not nM.
4. Degradation of the proteins was decreased from  $0.05 s^{-1}$  to  $10^{-4} s^{-1}$ .

After making the modifications, I observed similar results to the original paper. Although the absolute transcription rates were not comparable, the relative transcription rates appear similar to the published result. My simulation is shown in Figure 5 and a figure from the paper in Figure 6.

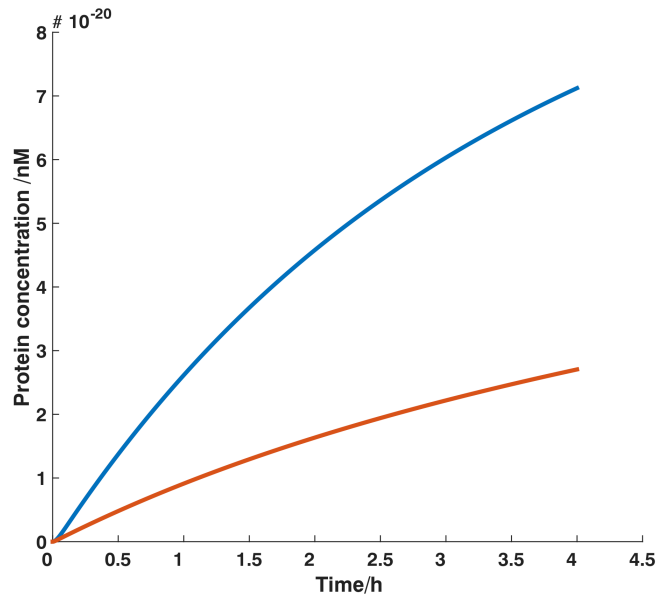


**Figure 5.** A simulation of protein expression. The concentration upstream gene is plotted and blue and the downstream gene in red.

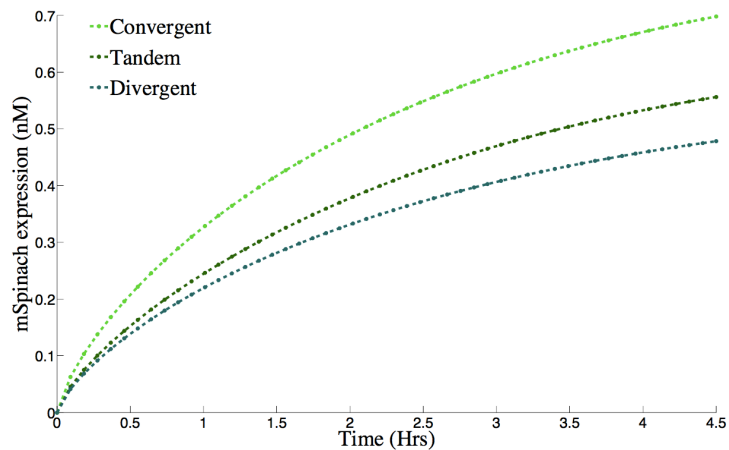


**Figure 6.** The downstream gene expression as presented in the original paper. I implemented the tandem model. Figure adapted from Yeung et al., 2014<sup>16</sup>.

### 5.3 Simulink

Dr Olivier Borkowski and I implemented the model in Simulink. We did this to find out whether we could achieve better results than from the Matlab code. There are two main advantages to using Simulink over Matlab. The first is the graphical representation of the model blocks. This reduces the chance of implementation errors. The other significant advantage is the use of the explicit Runge-Kutta method for solving differential equations. The Runge-Kutta method uses dynamic time steps to both minimise error and maximise computational efficiency. This method is superior in almost all areas compared to the Euler method, which I used in the Matlab code.

Even with the more advanced integrating method the results from the paper could not be reproduced completely. Like the Matlab model, the absolute values of transcription are different from the paper by a few orders of magnitude. Despite that, the shape, relative transcription rates and dynamics of the system are similar to those presented in the paper.

## 5.4 The insulator

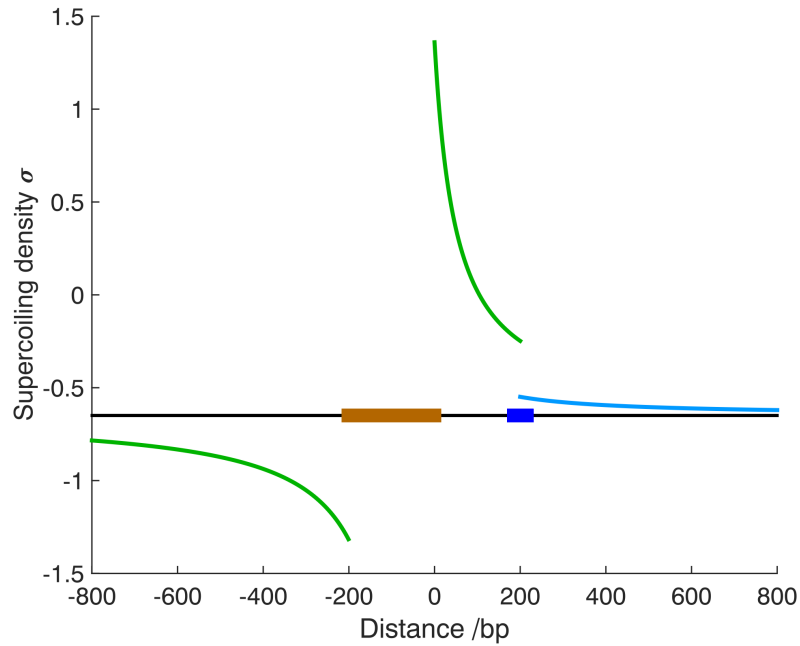
The only way to model the insulator is to understand its mechanism. I know that the insulator is a binding site for gyrase<sup>9,10</sup>. As discussed previously, gyrase relieves positive supercoils at a higher rate if the level of supercoiling is greater than  $\sigma_0$ . Taking this into account, along the location of insulator between the *gfp* and the terminator, I constructed a simple insulator model. The term that would be affected by the insulator addition was the first term of downstream promoter supercoiling: the effect from the upstream transcription complex. This models the fact that gyrase would be allowed to relieve local positive supercoiling to a much greater extent.

My first idea was to add a scaling factor to the term of interest. This extra parameter, called  $\alpha$ , would represent the ‘insulator effectiveness’, ranging from 0, a perfect insulator, to 1, no effect. However, this does not account for the gyrase binding events which vary with time. To model these events, I construct a binary function that takes the value of  $\rho$  when the gyrase is bound and 1 if unbound.  $\alpha$  can now be thought of as the insulator effectiveness as a function of time. We know that gyrase is activated when the supercoiling of a region is positive. This means that  $\alpha$  must also be a function of the local supercoiling level. Putting this all together gives:

$$\alpha(\rho, \sigma, t) = 1 - (1 - \rho)1_{\sigma > \sigma_0}f(t)$$

Where  $\rho$  is the intrinsic insulator effectiveness and  $0 \leq \rho \leq 1$ .  $f(t)$  can be any appropriate step function that outputs 1 when the gyrase is bound and 0 otherwise. I used a sine function with a threshold at  $\lambda$ . In other words when  $\lambda < \sin(\psi t)$ ,  $f(t)$  will be equal to 1 and  $\psi$  is the rate of binding events. It must also be noted that after inserting the insulator, the intergenic spacing will increase by the length of the insulator.

Testing the insulator proved to be an engaging task. The model is built in such a way that effect of the upstream transcription unit on the downstream promoter is negligible. Whether this is intentional or not is unknown. This can be seen by looking at the second term of the  $\sigma_{p,D}$  equation. The number of free ribosomes,  $R$ , will always be much greater than the number of transcription units at the upstream site. Removing or modifying the first term has virtually no effect on the simulation.



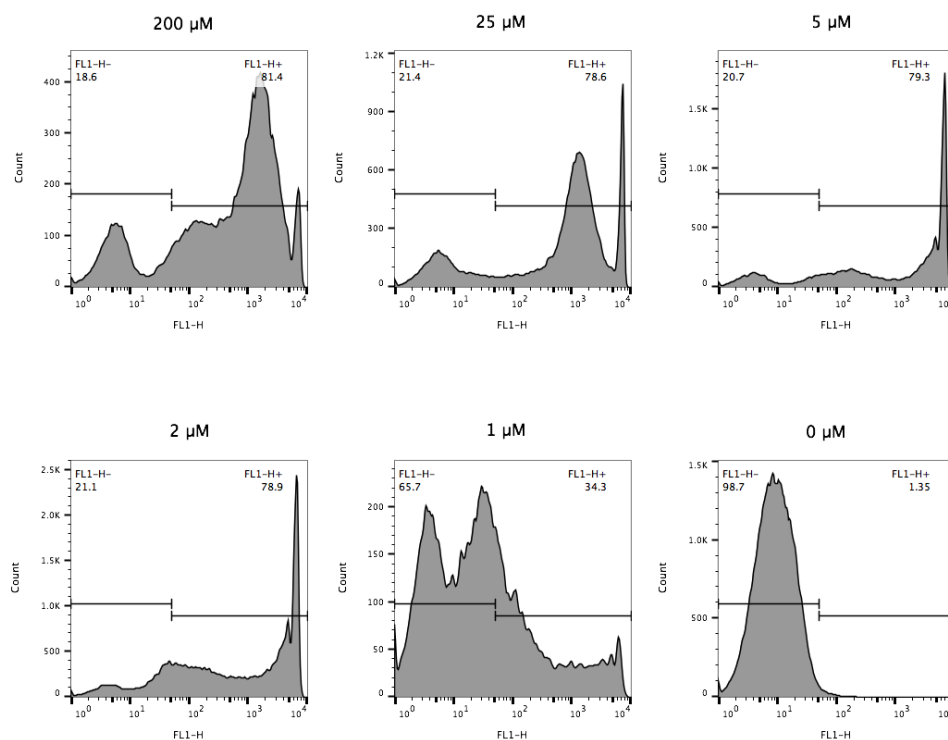
**Figure 7.** Simulation of the insulator (blue box) as a function of distance. The black line represents the DNA strand and the orange shape is a transcription site. The green lines indicate the level of supercoiling at each location. The blue line indicates the supercoiling level downstream of an insulator which is 80% effective. The natural supercoiling density of the *E. coli* genome is -0.65.

Figure 7 shows the insulator implemented in the part of the model that simulates the upstream transcription. In reality, and in the full model, the supercoiling level will fluctuate with time. This is a demonstration of the operation of the insulator. For the purposes of my model, I do not consider the upstream effects of the insulator. The green line should deform close to insulator and be continuous with the blue line.

## 6 Results

### 6.1 Generating supercoiling

The cultures were tested in a plate reader and  $OD_{600}$ , GFP and RFP is compared. All samples expressed GFP in the presence of arabinose. In the samples where arabinose concentration exceeded  $1 \mu\text{M}$  the GFP expression saturated the plate reader. This means that the stationary phase for these samples could not be captured using that method. The same samples were later tested in a flow cytometer to measure their GFP expression values.



**Figure 8.** Measurement of GFP expression with FACS (FL1-H channel) of the pGR-L3S2P21 plasmid at different arabinose concentrations. For every plot the cell populations are split into two, those expressing GFP and those that are not. The percentage of cells in each group can be seen in the upper corners of every graph.

A single sample for every plasmid at all arabinose concentration was tested in a flow cytometer. The results for GFP expression of pGR-L3S2P21 are plotted in Figure 8. As previously stated, I performed these tests in the DH10B strain. This strain sometimes exhibits a ‘binary switch’ property where beyond a certain level of induction a gene is maximally expressed. This could be the reason for cells at  $2 \mu\text{M}$  arabinose expressing similar GFP levels to those at higher arabinose concentrations. These results are consistent with the GFP plate reader measurements (not shown); where green fluorescence is not significantly expressed at  $0 \mu\text{M}$  and  $1 \mu\text{M}$  concentrations of arabinose; indicating that  $P_{\text{BAD}}$  is not remarkably induced.

With no arabinose present, there is a cell population that is not expressing GFP. At higher levels of arabinose, the populations are trimodal. A number of cells express very little or no fluorescence at any concentration. They are measured at between 0 and 50 (arb. fl. units). At  $2 \mu\text{M}$  and  $5 \mu\text{M}$  concentrations the majority of cells are expressing the green fluorescence at above 5000. At  $25 \mu\text{M}$  and  $50 \mu\text{M}$  the percentage of cells in the medium fluorescence expressing population (50 to 5000) are higher than at the

two lower concentrations. Nevertheless, 200  $\mu\text{M}$  of arabinose has the highest total percentage of cells expressing GFP at 81.4%.

## 6.2 Detecting supercoiling

In Figure 9 I compare the normalised RFP expression of pGR-L3S2P21 control plasmid, plotted in blue, with EAK-NG, in red. The results are from the plate reader (population). The six plots are at different arabinose concentrations. The control plasmid has no promoter driving RFP expression and hence low fluorescence is observed at all arabinose concentrations. EAK-NG is designed to respond to supercoiling and different concentrations of arabinose should result in variable RFP expressions. RFP activity appears to decrease slightly with higher arabinose concentrations. Due to the large errors at high concentrations, it is difficult to observe a trend. The steady state expression of EAK-NG is plotted in Figure 11.

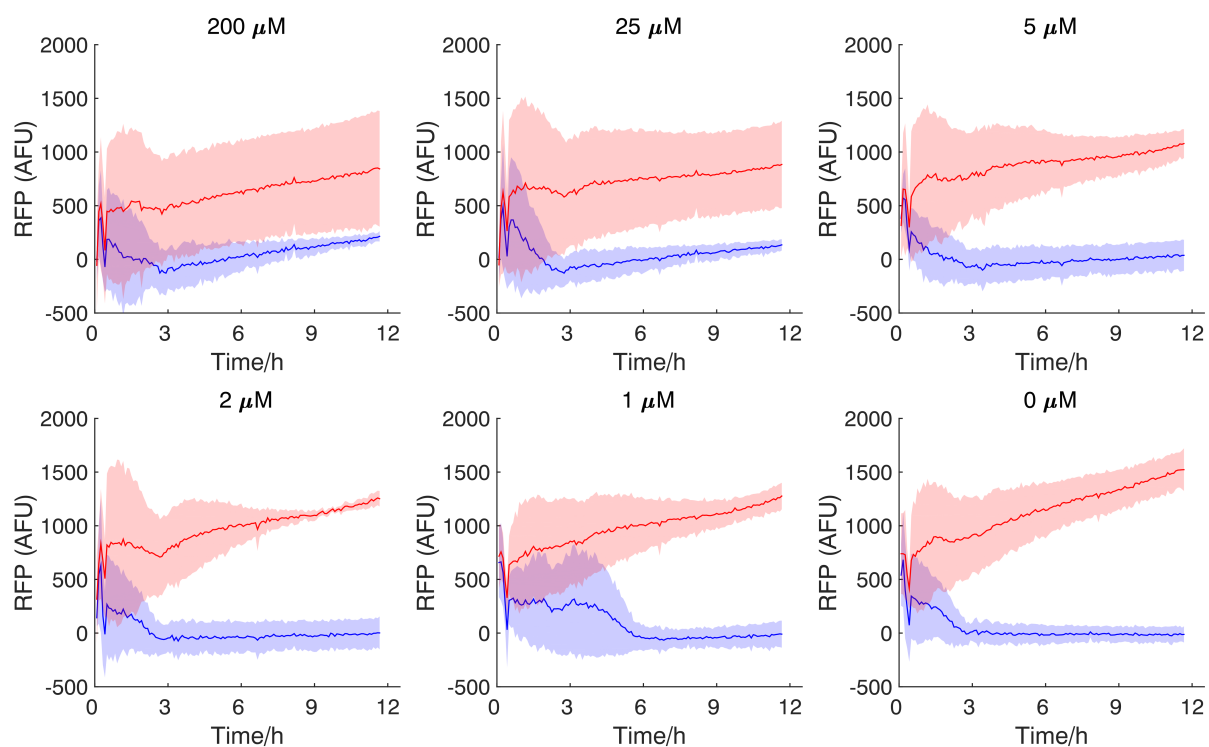


**Figure 9.** RFP expression of cultured cells as a function of time for different concentrations of arabinose. The control (pGR-L3S2P21) is plotted in blue and the supercoiling detector (EAK-NG) in red. Each line is the mean of four measurements done on different days. Shaded regions specify one standard deviation from the respective means.

The activity of  $P_{\text{gyrA}}$  in response to increased supercoiling levels has been shown to be a bell-shaped curve<sup>10</sup>. The peak of this curve, which was measured in a construct with driven by  $P_{\text{BAD}}$ , was at around 27  $\mu\text{M}$  concentration of arabinose. My results do not indicate this relationship. They indicate that there is no significant difference between  $P_{\text{gyrA}}$  activity at varying arabinose concentrations.

The small increase in expression of RFP measured in pGR-L3S2P21 at high arabinose values is probably due to the imperfect nature of the terminator. As transcription of the upstream *gfp* gene increases, the number of transcription complexes passing the terminator increases. This results in unwanted transcription of the downstream, *rfp* gene.

There are a number of factors that could lead to this result. Perhaps the  $P_{BAD-gfp}$  unit is not producing a measurable amount of supercoiling. This is unlikely as the  $P_{BAD}$  promoter has been used to generate supercoiling that affects  $P_{gyrA}$ <sup>10</sup>. However, that experiment used *uidA* as the reporter gene. It is possible that supercoiling that was detected in the experiment originated primarily from the transcription of *uidA* and not  $P_{BAD}$ . If *gfp* generates lower numbers of supercoils than *uidA* then this result could be partially explained.

Another possibility is that the *rfp* gene is very sensitive to the level supercoiling. If the expression of RFP decreases as supercoiling increases, it could counteract the increase in  $P_{gyrA}$ .

The irregular activity at the start could be traced to varying expression between samples in the exponential phase of cell growth.

### 6.3 Effect on constitutive promoter

Figure 10 shows the normalised RFP expression of the pGR-L3S2P21 plasmid, in blue, and EAK-NJ, in black. The control plasmid is the same as the one plotted above, in Figure 9. The six plots are at different arabinose concentrations. The *rfp* gene in EAK-NJ is controlled by a constitutive promoter. This promoter is not designed to respond to supercoiling.

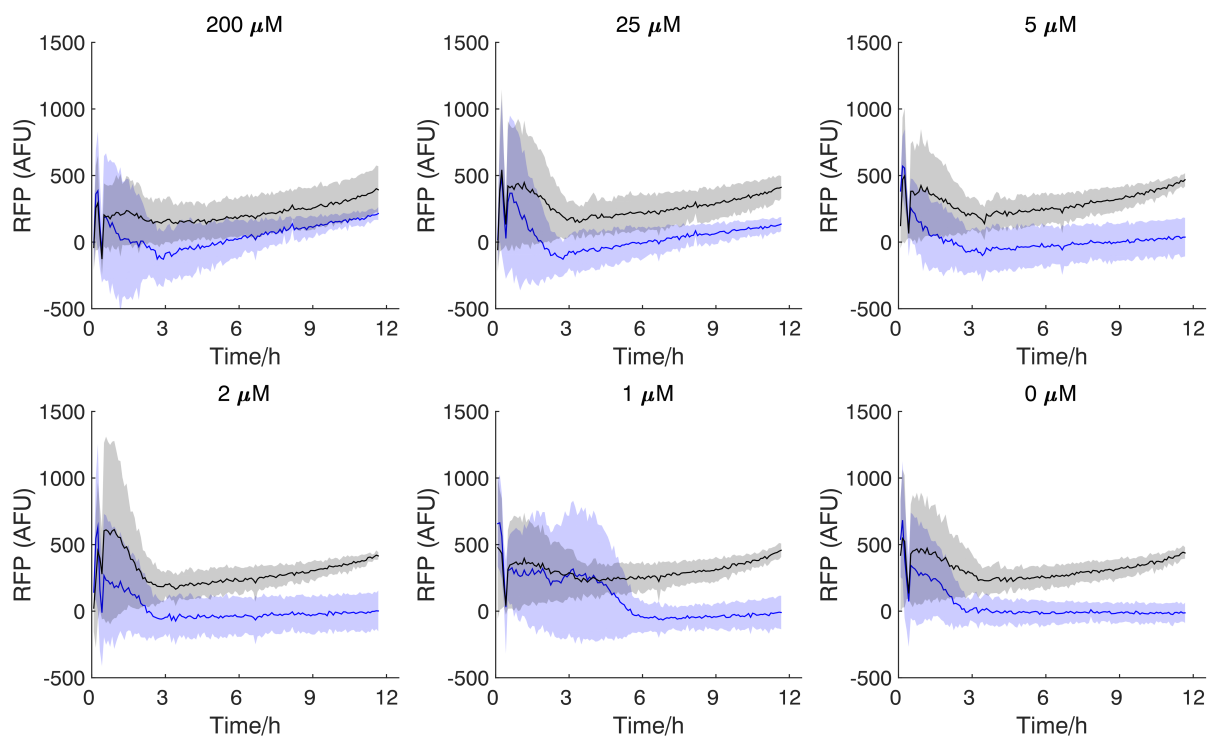


**Figure 10.** RFP expression as a function of time for different concentrations of arabinose. The control (pGR-L3S2P21) is plotted in blue and the constitutive promoter (EAK-NJ) in black. Each line is the mean of four measurements done on different days. Shaded regions specify one standard deviation from the respective means.

The absolute RFP expression of EAK-NJ remains constant at all arabinose levels. However, relative to the control plasmid, the constitutive promoter activity does not increase as much. As arabinose is increased, the difference between the two of them starts to become negligible. This is particularly noticeable at 200  $\mu$ M concentrations of arabinose. This could be the result of positive supercoiling

decreasing the downstream transcription rate, assuming constant terminator read-through. This reduction in expression could also be explained by the lack of available resources as GFP transcription is increased.

#### 6.4 The insulator

Figure 11 indicates that as arabinose concentration is increased the RFP expression of the plasmid (EAK-IG) carrying the insulator decreases. A bar graph was chosen over six separate line graphs, compare with previous graphs, for clarity. The decrease appears continuous with the exception of 1  $\mu\text{M}$  arabinose concentration. The uncertainty is quite significant and no conclusions can be drawn about the shape of the curve. However, it does look to be decreasing, particularly between 2  $\mu\text{M}$  and 200  $\mu\text{M}$ .

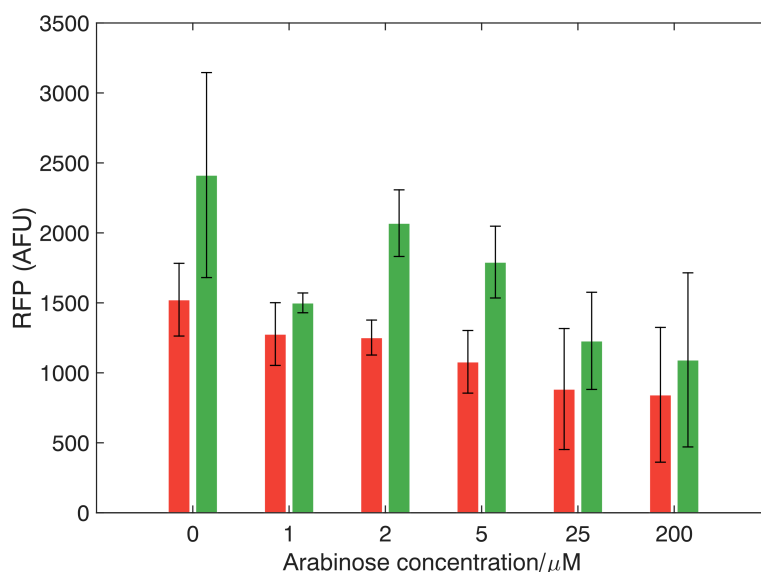


**Figure 11.** The normalised end-point RFP expression of the supercoiling detector plasmid (EAK-NG) in red, and EAK-IG, which contains the insulator, in green. Error bars indicate one standard deviation from the mean calculated from four measurements done on different days.

The insulator element did not behave as expected. At all tested concentrations of arabinose, the plasmid containing the insulator expressed higher levels of RFP than the plasmid that did not carry the insulator. This is inconsistent with other studies of this particular part<sup>10</sup>. However, the result of the plasmid without the insulator (EAK-NG) must be taken into account. Those measurements suggest  $P_{\text{gyrA}}$  activity might be slightly greater at low supercoiling levels. If the  $P_{\text{gyrA}}$  promoter is consistent between my plasmids, then it should follow that with the insulator added, its activity will not decrease.

#### 6.5 TX-TL

The three constructs were tested in a Rosetta BL21 based TX-TL system. Two separate experiments were conducted on different days. In both experiments, GFP expression was detected in most wells while RFP expression was not observed. The TX-TL system functions at much lower volumes than culture and consequently, the concentration of gyrase will be much higher. This could mean that the DNA is kept at supercoiled at a very different level, yet that does not explain the lack of RFP expression from the constitutive promoter.

## 7 Discussion

---

All plasmids contained the  $P_{BAD}$ -*gfp* unit. The green fluorescence measurements from the FACS indicate that I was able to control the induction of  $P_{BAD}$  by varying the concentration of arabinose. Although the control was not as precise as I had hoped, absence of arabinose clearly resulted in no fluorescence. One major setback was the saturation of the plate reader. During preliminary calibration trials on that plate reader I realised that some of the cultures expressed low levels of GFP and RFP. To increase the probability of capturing low expression I increased the gain of the plate reader to 60. This enabled me to observe the lower magnitudes of green fluorescence and unintentionally saturated the sensor. To achieve optimal performance, the entire range of GFP expression should be detected by the plate reader.

The GFP saturation issue was partially solved by measuring the same samples in a flow cytometer. One major advantage of FACS is that individual cells can be observed, as opposed to the weighted average of the population. This enabled me to detect bimodal and trimodal populations shown in Figure 8. RFP measurements were recorded in the FACS, but showed no variation between samples. The machine was set to maximum sensitivity, but could not discriminate between different levels. This could be because the frozen cultures were scratched with a tip and the concentration of cells was not high enough. Due to the time constraints of this project I was not able to measure the second plate with the FACS. More flow cytometry experiments are needed to convincingly quantify the fluorescence expression of the cell population. In light of the different measurement method between GFP and RFP and lack of repetition, I have decided that directly comparing them is not appropriate. I have omitted a plot of  $P_{BAD}$  and  $P_{gyrA}$  activity for this reason.

According to theory<sup>17</sup> and previous studies<sup>10,11</sup>, transcription of the upstream gene should generate supercoils that can diffuse past a terminator and affect local downstream transcription. My supercoiling reporter unit did not detect any significant changes in supercoiling when upstream transcription was active. This is most likely caused by one, or a combination, of the following scenarios.  $P_{gyrA}$  might not be sensitive to changes in supercoiling. This is contradicted by other studies<sup>10,11</sup> which show that  $P_{gyrA}$  activity does correlate with supercoiling. Therefore, I find it unlikely that this is the main source of error. Another possibility is that the translation of *rff* is inversely related to supercoiling density. The study<sup>10</sup> that inspired my experiments used *lacZ* as the reporter gene. It is possible that *lacZ* is inhibited less by supercoiling compared to *rff*. To test this theory *rff* could be substituted with *lacZ* in the EAK-NG plasmid. If *lacZ* expression changes with increased arabinose, then it is very likely that *rff* modulation was affecting the expression in cooperation with  $P_{gyrA}$ .

One of the questions I wanted to answer is whether supercoiling affects standard promoters. By standard promoters I am referring to promoters that would commonly be used in synthetic circuits. The promoter I tested, J23107, was chosen primarily because of its medium strength and lack of regulatory elements. This was done to minimise the effects of unintended induction and to make sure the promoter would not saturate. Figure 10 shows the results of the constitutive promoter experiments. The absolute RFP expressions controlled by J23107 remain comparatively constant at all arabinose concentrations. However, relative to the control plasmid, which has no constitutive promoter, the J23107 expression decreases. This could be due to supercoiling counteracting the effects of the terminator read-through.

The insulator element is a BIME-2 *nrdAB* site. This site has been demonstrated to act as a binding site for gyrase<sup>21</sup>. That means that this element has evolved to behave as a simple and very elegant natural insulator. Therefore, I find it very plausible that this element could serve the same purpose in synthetic circuits. As highlighted in the results, the insulator did not decrease the activity of  $P_{gyrA}$ , but these results

might not be representative as the  $P_{\text{gyrA}}$  displayed little change with arabinose concentration. In order to test the insulator properly, a promoter which exhibits quantified variation with supercoiling must be used.

One of the limitations of this insulator-element technique is the effect it has on the homeostatic regulation of gyrase. The aforementioned study<sup>21</sup> found 300 BIME sites in the *E. coli* chromosome. Adding more sites reduces the concentration of free gyrase, as more gyrase would be trapped in binding sites. This can affect gene expression because supercoiling density in the chromosome would be unevenly distributed<sup>11</sup>.

A secondary objective of this project was building and testing a TX-TL system. Since the conditions of TX-TL are not the same as *in vivo*, the results will not match perfectly. For many purposes those differences are negligible and TX-TL can work as a substitute for culture experiments<sup>6</sup>. However, I was not able to replicate my culture experiments in TX-TL. It must be noted that system is new and has not been implemented in this lab before. Many experimental parameters, such as buffer concentration, are unique to each batch and may require further tuning<sup>13</sup>.

Gyrase might behave differently than in culture, particularly as it occurs in higher concentrations. Further studies into the effects of gyrase in TX-TL systems are required. An alternative theory for the disparity could be the RFP expressed by the *rfp* gene. RFP is a more complex molecule and folds at a slower rate than GFP. In TX-TL reactions typically last around four hours. Perhaps this is not enough time for the RFP to always mature.

To improve the TX-TL model presented in Yeung et al., 2014<sup>16</sup>, which I implemented, the parameters will have to be more accurately quantified. Small changes to initial conditions cause very large differences in the output. The insulator model will also have to be compared with the results from the EAK-IJ plasmid. Hopefully it will be possible to assign a value to the efficiency of the insulator. Without a working construct with a constitutive promoter and insulator for testing and validation, the model could not be developed further.

## 8 Conclusion

---

In this project, I set out to answer three questions: Can supercoiling be quantified? Does supercoiling affect transcription? And is it possible to modulate supercoiling effects? I designed four plasmids to answer these questions. Out of those four, three were successfully constructed and tested. The first plasmid (EAK-NG) was designed to generate and detect supercoiling. The second plasmid (EAK-IG) was designed to test an insulator element. This element can possibly focus the action of gyrase to relieve negative supercoils in a specific region. The third plasmid (EAK-NJ) contained a constitutive promoter instead of  $P_{gyrA}$ . I used this plasmid to investigate the effects of supercoiling on transcription.

In culture, the GFP expression saturated the plate reader sensor due to the gain being too high. After measuring the same sample using FACS, I confirmed the activation of  $P_{BAD}$ . Comparing RFP expressions, I found no significant correlation between the induction of  $P_{BAD}$  and the activity of  $P_{gyrA}$ . This conflicts with previous studies and must be investigated further. The RFP expression of EAK-NJ decreased relative to the control plasmid. This could be due to TI supercoils diffusing to the downstream transcription site, assuming that terminator read-through is the same in both plasmids. The plasmid containing the insulator displayed higher levels of RFP than the plasmid that did not contain the insulator. This was opposite to what I expected to find. Considering the fact that  $P_{gyrA}$  activity did not increase with supercoiling, I cannot rule out the possibility that the insulator worked. After assembling the TX-TL system I tested the same circuits. The wells that contained arabinose and the  $P_{BAD}$  part expressed some GFP, while none of the constructs appeared to express the *rfb* gene.

EAK-IJ was the fourth plasmid that I designed. I planned on comparing the result of this plasmid with EAK-NJ to further study the effect of the insulator. Unfortunately, this plasmid could not be realised despite adhering to good laboratory practices. After two attempts, sequencing confirmed that the cloning had not been successful. I implemented a supercoiling model for TX-TL in Matlab. Due to simulation issues with the model, I was required to make some modifications. This meant I was not able to recreate the model fully, but some of the discrepancies might be due to my use of the Euler integration method. However, the same model could not be implemented with the dynamic Runge-Kutta method in Simulink. I modelled the insulator element and integrated it into the existing model. The insulator model works as designed when simulating spatial supercoiling density with respect to one transcription site.

Additional work that addresses the limitations of this project is warranted. My thoughts on further studies related to DNA supercoiling are detailed in the next chapter.

## 9 Future work

---

### 9.1 Distance

An interesting topic that was not part of this project is the diffusion of supercoiling as a function of distance. We know that TI supercoiling returns to the natural level as distance from the transcription site increases<sup>10,16</sup>. Perhaps increasing the distance alone is sufficient to avoid variations in local TI supercoiling. Should this be the case it could turn out more reliable than the current insulator element design. This stems from the fact that the insulator element relies on gyrase to correct the supercoiling level. Hence, the effectiveness of the element is a function of gyrase concentration and availability.

The aforementioned study claims that supercoiling diffuses at least 6 kb away from the transcription site. According to the Yeung model<sup>16</sup>, moderate levels of supercoiling propagate to around 1 kb from the site of transcription. To test the range of TI supercoiling effects a series of constructs could be built, based on EAK-NG, one made for this project. The difference would be the distance between the upstream supercoiling generation complex and the downstream detection complex. The sequence would have to be noncoding to ensure no transcription events occur between the generator and the detector.

Another interesting question is whether the sequence of this noncoding DNA code ‘buffer’ is important. Since guanine-cytosine bonds contain three hydrogen bonds, as opposed to two in adenine-thymine bonds, they deform slightly differently. Perhaps GC-rich sequences inhibit TI supercoiling better than GC-poor sequences. Alternatively, GC-poor sequences might be more flexible and hence absorb supercoiling to a greater degree. This leads to yet another question: is it conceivable that noncoding DNA parts have evolved, to some extent, as natural supercoiling insulators?

### 9.2 The improved insulator

A drawback of the current insulator element is that it could possibly interfere with the natural messenger system that has been suggested<sup>11</sup>. An insulator would effectively cut one or more of the connections in this network with unknown consequences. A better solution would be to detect the supercoiling before the insulator and generate the same level downstream of the parts that require isolation. This could be achieved using a small signalling network where the supercoiling detector unit expresses a concentration of a molecule that correlates with the level of supercoiling. The downstream generator unit then recognises this molecule and produces supercoiling to the appropriate degree.

### 9.3 Supercoiling map

A catalogue of supercoiling sensitive genes (SSGs) have already been mapped onto the genome of *E. coli*, Figure 12<sup>11</sup>. I think it would be interesting to build on this in two ways. Firstly, a system that would check if an insert is being cloned inside the sensitive range of an SSG. This could be integrated into a DNA cloning system, like Benchling, to warn about potential interference with supercoiling sensitive housekeeping or regulatory genes.

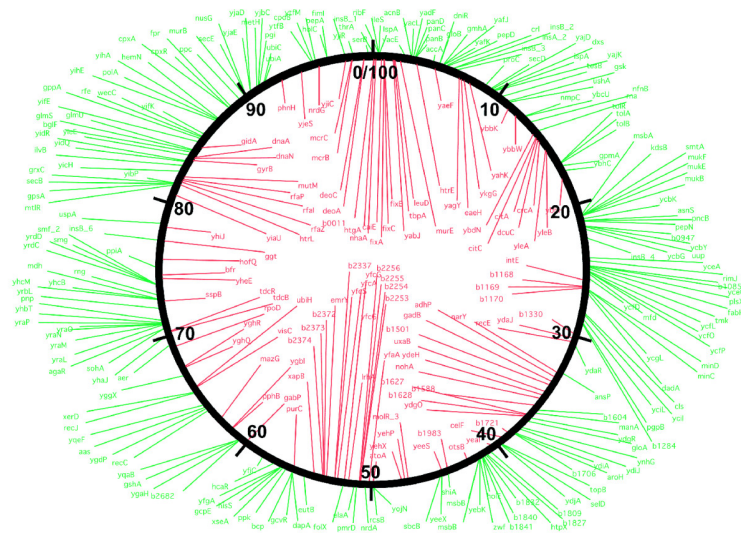


**Figure 12.** SSGs mapped onto the *E. coli* genome. A similar map, but showing the variation in supercoiling would be helpful. Figure adapted from Peter et al, 2004<sup>11</sup>.

The second type of map would be the supercoiling variation in the entire genome. Regions where supercoiling is highly variable could be avoided. This would help with implementing sensitive parts or circuits.

## 10 Acknowledgements

---

Special thanks to Dr Olivier Borkowski for his help and guidance throughout the whole project, and for letting me use part of his bench space. I would like to thank Dr Tom Ellis for his ideas and giving me the opportunity to work on this project. Finally, thanks to the entire Ellis lab for their good advice and assistance, in particular Dr Ben Blount for helping me set up and use the flow cytometer.

## 11 References

---

1. Nirenberg, M. W., & Matthaei, J. H. (1961). The dependence of cell-free protein synthesis in *E. coli* upon naturally occurring or synthetic polyribonucleotides. *Proceedings of the National Academy of Sciences of the United States of America*, *47*(10), 1588–1602. Retrieved from <http://www.ncbi.nlm.nih.gov/pmc/articles/PMC223178/>
2. Katzen, F., Chang, G., & Kudlicki, W. (2005). The past, present and future of cell-free protein synthesis. *Trends in Biotechnology*, *23*(3), 150–156. doi:10.1016/j.tibtech.2005.01.003
3. Siegal-Gaskins, D., Tuza, Z. A., Kim, J., Noireaux, V., & Murray, R. M. (2014). Resource usage and gene circuit performance characterization in a cell-free “breadboard.” *ACS Synthetic Biology*. doi:10.1021/sb400203p
4. Michel, E., & Wüthrich, K. (2012). High-yield *Escherichia coli*-based cell-free expression of human proteins. *Journal of Biomolecular NMR*, *53*(1), 43–51. doi:10.1007/s10858-012-9619-4
5. Zhang, Y. H. P., Evans, B. R., Mielenz, J. R., Hopkins, R. C., & Adams, M. W. W. (2007). High-yield hydrogen production from starch and water by a synthetic enzymatic pathway. *PLoS ONE*, *2*(5), 2–7. doi:10.1371/journal.pone.0000456
6. Shin, J., & Noireaux, V. (2012). An *E. coli* cell-free expression toolbox: Application to synthetic gene circuits and artificial cells. *ACS Synthetic Biology*, *1*, 29–41. doi:10.1021/sb200016s
7. Nelson, P. (1999). Transport of torsional stress in DNA. *Proceedings of the National Academy of Sciences of the United States of America*, *96*(25), 14342–14347. doi:10.1073/pnas.96.25.14342
8. Vos, S. M., Tretter, E. M., Schmidt, B. H., & Berger, J. M. (2011). All tangled up: how cells direct, manage and exploit topoisomerase function. *Nature Reviews Molecular Cell Biology*, *12*(12), 827–841. doi:10.1038/nrm3228
9. Menzel, R., & Gellert, M. (1983). Regulation of the genes for *E. coli* DNA gyrase: homeostatic control of DNA supercoiling. *Cell*, *34*(1), 105–113. doi:http://dx.doi.org/10.1016/0092-8674(83)90140-X
10. Moulin, L., Rahmouni, a. R., & Boccard, F. (2005). Topological insulators inhibit diffusion of transcription-induced positive supercoils in the chromosome of *Escherichia coli*. *Molecular Microbiology*, *55*, 601–610. doi:10.1111/j.1365-2958.2004.04411.x
11. Peter, B. J., Arsuaga, J., Breier, A. M., Khodursky, A. B., Brown, P. O., & Cozzarelli, N. R. (2004). Genomic transcriptional response to loss of chromosomal supercoiling in *Escherichia coli*. *Genome Biology*, *5*, R87. doi:10.1186/gb-2004-5-11-r87
12. Chen, Y.-J., Liu, P., Nielsen, A. a K., Brophy, J. a N., Clancy, K., Peterson, T., & Voigt, C. a. (2013). Characterization of 582 natural and synthetic terminators and quantification of their design constraints. *Nature Methods*, *10*(7), 659–64. doi:10.1038/nmeth.2515
13. Sun, Z. Z., Hayes, C. a, Shin, J., Caschera, F., Murray, R. M., & Noireaux, V. (2013). Protocols for implementing an *Escherichia coli* based TX-TL cell-free expression system for synthetic biology. *Journal of Visualized Experiments: JoVE*, (September), e50762. doi:10.3791/50762
14. Chung, C. T., & Miller, R. H. (1993). Preparation and storage of competent *Escherichia coli* cells. *Methods in Enzymology*, *218*(1979), 621–627. doi:10.1016/0076-6879(93)18045-E

15. Gibson, D. G., Young, L., Chuang, R.-Y., Venter, J. C., Hutchison, C. a, & Smith, H. O. (2009). Enzymatic assembly of DNA molecules up to several hundred kilobases. *Nature Methods*, 6(5), 343–345. doi:10.1038/nmeth.1318
16. Yeung, E., Ng, A., Kim, J., Sun, Z. Z., & Murray, R. M. (2014). Modeling the Effects of Compositional Context on Promoter Activity in an E. Coli Extract based Transcription-Translation System, (Cdc).
17. Liu, L. F., & Wang, J. C. (1987). Supercoiling of the DNA template during transcription. *Proceedings of the National Academy of Sciences of the United States of America*, 84(October), 7024–7027. doi:10.1073/pnas.84.20.7024
18. Kolbeinsson, Arinbjörn. *Cell-free and supercoiling – Interim report*. 2015.
19. Pruss, G. J., & Drlicat, K. (1988). DNA Supercoiling and Prokaryotic Transcription Minireview. *Cell*, 56, 521–523.
20. Sun, Z. Z., Yeung, E., Hayes, C. a., Noireaux, V., & Murray, R. M. (2014). Linear DNA for rapid prototyping of synthetic biological circuits in an escherichia coli based TX-TL cell-free system. *ACS Synthetic Biology*, 3, 387–397. doi:10.1021/sb400131a
21. Espéli, O., & Boccard, F. (1997). In vivo cleavage of Escherichia coli BIME-2 repeats by DNA gyrase: genetic characterization of the target and identification of the cut site. *Molecular Microbiology*, 26(4), 767–777.
22. Kearney, K. Boundedline.m v1.4. Covered by the MIT licence. Retrieved from <http://www.mathworks.com/matlabcentral/fileexchange/27485-boundedline-m>
23. Callaghan, M. Barwitherr v1.12. Covered by BSD licence. Retrieved from <http://uk.mathworks.com/matlabcentral/fileexchange/30639-barwitherr-errors-varargin->

## 12 Appendix

### 12.1 List of primers

**Table 9.** Primers used in this project

Name	Sequence
pGR-L3S2P21_part1 FWD	AGTAGAGGGATAGCGGTTAGATGGCTTCCTCCGAAGACGT
pGR-L3S2P21_part1 REV	CATCCGGCATCTCAATATCATTATTATTTGTATAGTTCATCCATGCCA
Insulator FWD	ATGAACTATACAAATAATAATGATATTGAGATGCCGGATG
Insulator REV	AATTTGGTACCGAGGAATTCTTAATGCCGATAAAGGCATT
PgyrA FWD	AGAAAGAGGAGAAATACTAGCATTGGATGTGAATAAAGCG
PgyrA REV	ACGTCTTCGGAGGAAGCCATCTAACCGCTATCCCTCTACT
pGR-L3S2P21_terminator FWD	AATGCCTTATCCGGCATTAGAATTCTCGGTACCAAATT
pGR-L3S2P21_terminator REV	CGCTTTATTCACATCCAATGCTAGTATTTCTCCTCTTTCTG
OB_Supercoiling_insulator_plasmid FWD	GCCCTAGGTATTATGCTAGCATGGCTTCCTCCGAAGACGT
OB_Supercoiling_insulator_plasmid REV	AGGGCTGAGCTAGCCGTAAACTAGTATTTCTCCTCTTTCTGCAGC
OB_J23107 FWD	AGAAAGAGGAGAAATACTAGTTTACGGCTAGCTCAGCCCT
OB_J23107 REV	ACGTCTTCGGAGGAAGCCATGCTAGCATAATACCTAGGGCT

### 12.2 Program code

The following code is the Matlab implementation of the Yeung et al., 2014<sup>16</sup> model.

```
% Supercoiling model
% Arinbjorn Kolbeinsson
% Imperial College London
% 2015

% Equations adapted from "Modeling the Effects of Compositional Context on Promoter
Activity in an E. coli Extract based Transcription-Translation System" Enoch Yeung,
Andrew Ng, Jongmin Kim,
% Zachary Z. Sun, and Richard M. Murray. 2014.
% http://www.cds.caltech.edu/~murray/papers/yeu+14-cdc.html

%% Parameters
delta = 0.036; %step size (seconds)
T = 400000; %number of cycles
h0 = 10.5;
tau = 0.25;
gamma = 0.5;
sigma_0 = -0.65;
deg_m = 0.0001;
omega = 7.85*10^11;
TL_S = 681;
TL_G = 720;
PL_S = 101;
PL_G = 1210;
NS = 105;
```

Continued on next page...

```

kf_max = 10^-5;
kcat_max = 5.4*10^-4;
k_w = 10^-9;
k_l = 0.02;
k_r = 0.01;

%Initial conditions
sigma_tS = -0.65;
sigma_tG = -0.65;
sigma_pS = -0.65;
sigma_pG = -0.65;
mS = 0;
MG = 0;
k_seq = 1;
EC_S = 0;
EC_G = 0;
ECGECS = 0;
R_tot = 10^-6 - EC_S + EC_G + ECGECS;
PLac_tot = 11*10^-9;
PTet_tot = 11*10^-9;

%Rate dynamics
for i=1:T

if(sigma_tS(i)>sigma_0)BtS = -gamma;
else BtS = tau;
end
if(sigma_pG(i)>sigma_0)BpG = -gamma;
else BpG = tau;
end
if(sigma_pS(i)>sigma_0)BpS = -gamma;
else BpS = tau;
end
if(sigma_tG(i)>sigma_0)BtG = -gamma;
else BtG = tau;
end

PLac(i) = PLac_tot - EC_S(i) - ECGECS(i);
PTet(i) = PTet_tot - EC_G(i) - ECGECS(i);

sigma_tS(i+1) = sigma_tS(i) + (delta)*(-(omega/2)*(kcat(sigma_tS(i), kcat_max,
TL_S)*EC_S(i) ) + (h0/TL_S)*BtS );
sigma_pG(i+1) = sigma_pG(i) + delta*(-(omega/2)*(kf(sigma_pG(i),
kf_max)*PTet(i)*(R_tot - (EC_S(i) + EC_G(i) + ECGECS(i)))) + (h0/PL_G)*BpG);

sigma_pS(i+1) = sigma_pS(i) + delta*((omega/2)*(kcat(sigma_pG(i), kcat_max,
TL_G)*EC_G(i)*(TL_G/(2*(PL_S+NS))) - kf(sigma_pS(i), kf_max)*PLac(i)*(R_tot -
(EC_S(i) + EC_G(i) + ECGECS(i)))-kcat(sigma_tS(i), kcat_max,
TL_G)*EC_S(i)*(TL_G/(PL_S+NS))) + (h0/PL_S)*BpS);
sigma_tG(i+1) = sigma_tG(i) + delta*( -(omega/2)*(kcat(sigma_tS(i), kcat_max,
TL_S)*EC_S(i)*(TL_S/(PL_S+NS+TL_G+TL_S)) + kcat(sigma_tG(i), kcat_max,
TL_G)*EC_G(i) + kf(sigma_pS(i), kf_max)*PLac(i)*(R_tot - (EC_S(i) + EC_G(i) +
ECGECS(i)))*(PL_S/(2*(TL_G+NS)))) + (h0/TL_S)*BtG);

mS(i+1) = mS(i) + (delta)*(kcat(sigma_tS(i), kcat_max, TL_S)*EC_S(i)+k_w*ECGECS(i)-
deg_m*mS(i));
MG(i+1) = MG(i) + delta*(kcat(sigma_tG(i), kcat_max, TL_S)*EC_G(i)+k_w*ECGECS(i)-
deg_m*MG(i));
EC_S(i+1) = EC_S(i) + (delta)*(kf(sigma_pS(i), kf_max)*(R_tot - (EC_S(i) + EC_G(i)
+ ECGECS(i)))*PLac(i)-(k_r+kcat(sigma_tS(i), kcat_max, TL_S))*EC_S(i));
EC_G(i+1) = EC_G(i) + (delta)*(kf(sigma_pG(i), kf_max)*(R_tot - (EC_S(i) + EC_G(i)
+ ECGECS(i)))*PTet(i)-(k_r+kcat(sigma_tG(i), kcat_max,
TL_G)+kseq(sigma_tG(i))+k_l)*EC_G(i));
ECGECS(i+1) = ECGECS(i) + (delta)*(k_l*EC_G(i) - k_w*ECGECS(i));
end

```

Continued on next page...

```

figure;
%subplot(2,2,1);
hold on;
plot(mS, 'LineWidth',4);
plot(MG, 'LineWidth',4);
    xlab = 0:0.5:4.5;
    xp = xlab*12;

    set(gca, 'XTickLabel',xlab); % Change x-axis ticks labels to desired values.
    xlabel('Time/h') % x-axis label
    ylabel('Protein concentration /nM') % y-axis label
    set(gca, 'FontSize',18, 'FontWeight', 'bold')

```

The accompanying functions are listed below.

```

function [ out ] = kcat( sigma, max, TL )
%function accompanies supercoilingGFPRFP.m

out = (max/TL)/(abs(sigma+0.65)+1);

end

```

```

function [ out ] = kf( sigma, max )
%function accompanies supercoilingGFPRFP.m

out = max/(abs(sigma+0.65)+1);

end

```

```

function [ out ] = kseq( sigma )
%function accompanies supercoilingGFPRFP.m

s_0 = -0.65;

if(sigma<s_0)
    out = abs(sigma-s_0)/(1+abs(sigma-s_0));
else
    out = 0;

end

```